Materials Science in Semiconductor Processing 219 (2027) 111333

Contents lists available at ScienceDirect

Materials Science in Semiconductor Processing

journal homepage: www.elsevier.com/locate/mssp

Infrared properties of a highly compensated germanium doped with shallow donors and acceptors below the Mott transition

S.G. Pavlov [a,*], N.V. Abrosimov [b], D.L. Kamenskyi [c], H.-W. Hübers [a,c]

[a] Institute of Space Research, German Aerospace Center (DLR), Berlin, Germany
[b] Leibniz-Institut für Kristallzüchtung (IKZ), Berlin, Germany
[c] Institut für Physik, Humboldt-Universität zu Berlin, Berlin, Germany

ARTICLE INFO

Keywords:
Compensation
Germanium
Infrared spectroscopy

ABSTRACT

Highly compensated germanium crystals doped closely to the partial Mott transitions of donors and acceptors have been produced and investigated by conventional analytics to determine concentration of electrically and optically active charge centers at various temperatures. Electric measurements reveal the net active concentration in compensated, gradient-doped *n*-type and *p*-type germanium crystals, co-doped with a targeted antimony and gallium along the growth axis. Infrared absorption spectroscopy shows gradual changes in far-infrared absorption depending on the degree of compensation and the lattice temperature. This absorption can be modulated by an external light source, whose photons provide photoionization across the band gap. At lattice temperatures, corresponding to the freeze-out of free charge carriers onto Coulomb impurity centers, far-infrared absorption increases within a broad spectral band, with a maximum at approximately at the binding energy of the dopant. Such materials are suitable for a wide range of applications requiring control over of concentration, capture rates and optical absorption of free charge carriers in semiconductors.

1. Introduction

Compensation engineering of elemental semiconductors offers a versatile material for specialized, high-performance technological applications, among those fast, spectrally-broadened and quantum-level (opto)electronics, see e.g. Refs. [1–6]. Near-perfect compensation is used to create semi-insulating materials (such as silicon, SiC or GaAs) to provide highly resistive, isolated substrates for high-frequency integrated circuits. As a rule, the compensating impurity with a larger binding energy than that of the dominant dopant is selected; in this case, the dominant physical mechanism is attributed to interband recombination, commonly explained within the framework of Shockley-Read-Hall recombination theory [4]. Using deep centers, one can provide pinning of the Fermi level near the middle of the band gap, thereby significantly reducing the concentration of free charge carriers in the semiconductor – a commonly used approach for minimizing microwave losses in the optical windows of high-power devices such as gyrotrons [5]. Hopping conductivity, occurring in highly-doped and compensated semiconductors, can potentially be used for optimization of light absorption in far-infrared bolometers based on compensated germanium/silicon due to enhancement of hopping conductivity [6]. Controlling compensation in moderately doped germanium (Ge) crystals enables fast recovery of the photoionized impurities, thereby facilitating the ultra-fast detection of infrared pulses from free-electron laser [2]. For applications in the far-infrared (terahertz frequency) range requiring low-loss, sensitive and spectrally broad-band sensing [7], materials combining low static infrared losses with high concentrations of dynamic free charge carriers, are desirable.

The primary objective of this study was to develop a material which capable of deep modulation of transmitted light - exclusively, in the far-infrared wavelength range. For this purpose, we select, as the matrix, germanium crystals, known to exhibit very low lattice absorption in this spectral range [8]. Impurity-to-band transitions, which exhibit the largest absorption cross section in the target spectral range, have been chosen to provide optical losses. To achieve their fast, effective modulation, we consider the band-gap light ($> E_g \approx 0.66$ eV or < 1.9 μm), which modifies the populations of impurity ground states, assuming their fast repopulation via free carriers captured from the conduction

This article is part of a special issue entitled: GADEST 2026 published in Materials Science in Semiconductor Processing.

* Corresponding author.
E-mail addresses: sergeij.pavlov@dlr.de (S.G. Pavlov), nikolay.abrosimov@ikz-berlin.de (N.V. Abrosimov), Dmytro.Kamenskyi@dlr.de (D.L. Kamenskyi), heinz-wilhelm.huebers@dlr.de (H.-W. Hübers).

https://doi.org/10.1016/j.mssp.2026.111333
Received 22 June 2026; Received in revised form 8 October 2026; Accepted 21 October 2026
Available online 24 October 2026
1369-8001/© 2026 German Aerospace Center, Institute of Space Research, Berlin, Germany. Published by Elsevier Ltd. This is an open access article under the CC BY license (http://creativecommons.org/licenses/by/4.0/).
Open access funding enabled and organized by Projekt DEAL.

and valence bands. This is organized, in turn, employing highly compensated crystals (degree k = minor/major dopant), whose density of charged Coulomb centers should provide fast capture of the band-gap photoionized carriers onto impurity centers, dominantly to their inter-band recombination (Fig. 1). The use of donor and acceptor center with approximately equal binding energies (0.0103 eV and 0.0113 eV) ensures their matched thermal activation temperatures as well as nearly identical impurity-to-band far-infrared spectra. Consequently, highly-doped and highly compensated (HDHC) germanium crystal with shallow donors and acceptors must be made for this goal. Targeted co-doping during the Czochralski crystal growth process, makes it possible to obtain high-quality homogeneous distributions of the desired impurities in Ge crystals.

The doping level was selected by trade-off between significant impurity-to-band absorption and potential losses induced by inhomogeneous doping. The latter can cause percolation effects arising from random fluctuations in the electrostatic potential, which could otherwise cause additional, persistent losses [9]. A further limitation arises from the effect of impurity bands, that are formed of merged impurity states at high dopant densities in HD Ge - including the ground state of the dopants. In a uniformly compensated HD semiconductor, the factor $N^{1/3}\bullet a^*$, related to the total defect' concentration and the mean state radius, describes a regime of strong spatial overlap of localized states [9]. The empiric values of the semiconductor-metallic, Mott transition, expected at $N_M^{1/3}\bullet a^*_B > 0.25$ (a^*_B is the effective Bohr radius, which can be viewed as the mean radius of the impurity ground state), have been determined for shallow impurities in Ge as: $N_{Sb\ (M)} \approx (0.95\text{-}1.55)\bullet 10^{17}$ cm^{-3} [10,11]; $N_{Ga(M)} \approx (1.0\text{-}1.86(1))\bullet 10^{17}$ cm^{-3} [12,13]. Assuming that the radii of excited, Rydberg-like impurity states scale with their binding energies, the lowest excited states (the binding energy of 4.75 and 4.6 meV) should overlap beginning from approximately (1.-1.5)$\bullet 10^{16}$ cm^{-3}. In this scenario of only ground impurity state remaining isolated, the sum concentration of Sb and Ga can be selected within the range (1.-9.)$\bullet 10^{16}$ cm^{-3}.

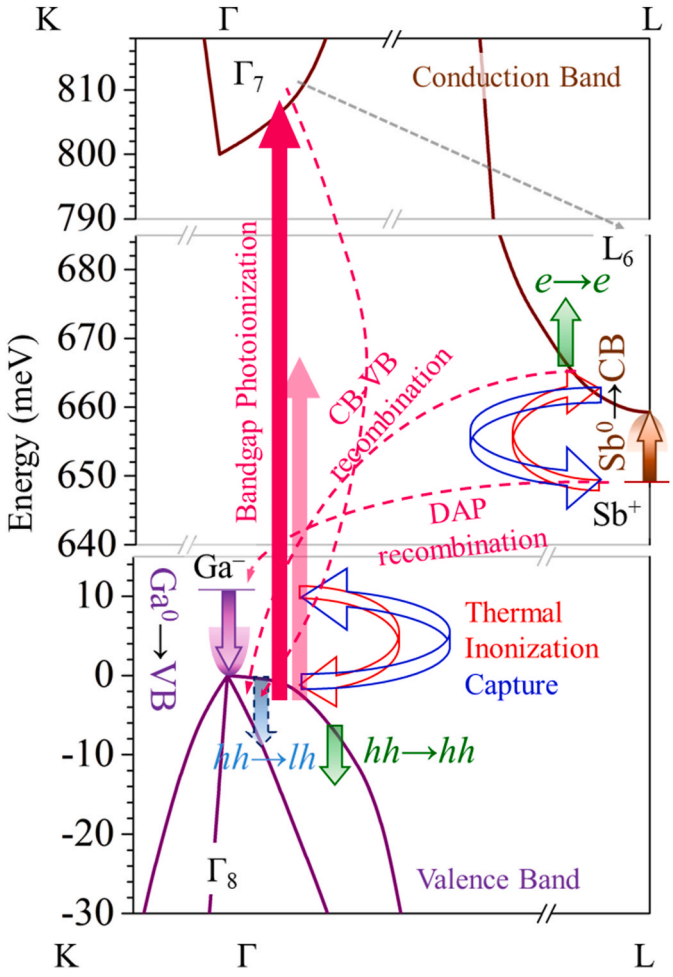


Fig. 1. Schematic representation of the electronic states and processes determining far-infrared absorption in compensated germanium. Gallium and antimony symbols denote the localized levels (ground states) of shallow impurities; the bold, straight arrows near them represent far-infrared absorption: intra-center photoexcitation (Ga^0/Sb^0: ground state → excited states), and impurity → band (Ga^0 → VB, Sb^0 → CB) photoionization processes. Other far-infrared absorption processes are of intraband types, within the same (sub)band (CB: e → e; VB: hh → hh; lh → lh) and intersubband (VB: hh → lh). Interband (CB-VB) and Donor-Acceptor pair (DAP) recombinations are shown with dashed arrows. Thermal ionization at high lattice temperature and capture into the ground state of impurity centers at low temperatures are shown with hollow arrows. The upward arrows in the center show broadband excitation, including the direct and indirect interband photons. A diagonal dashed arrow within the conduction band indicates intervalley scattering (Γ → L) of photoinduced free electrons.

A HC semiconductor has almost equal concentrations of donors and acceptors $N_D \approx N_A$. Through the complete donor-acceptor recombination of charge carriers, - which originally were bound to their neutral impurity atoms, - both the donor and acceptor centers (Sb^0, Ga^0) become charged, positively (Sb^+) and negatively (Ga^-), respectively (Fig. 1). Intracenter and impurity-band light absorption processes are cancelled for ionized impurities, while the free charge carrier concentration approaches the net concentration $|N_D - N_A|$. The Fermi level is pinned near the middle of the band gap ($E_g/2$), and the material exhibits properties resembling those of a net doped (like a low-doped at large k) semiconductor. Reduced density of free carriers in HC Ge results in low-level far-infrared absorption at temperatures well above the binding energies of the present impurity centers, when impurity-to-band absorption is cancelled. Far-infrared absorption should arise from weak Drude-type process (Fig. 1), as well as lattice modes via second-order difference-phonon processes [8]. Similarly, low far-infrared absorption was expected to appear in HC Ge at low lattice temperatures, when compensation maintains a balance of ionized impurity centers, while lattice absorption decreases significantly due to the reduced densities of thermal phonons [8]. The strength of impurity-to-band absorption should be controllable via the intensity of external light source. When band-gap light illuminates the material, it generates free electron-hole pairs. These photogenerated minority carriers are rapidly captured by the oppositely charged impurity centers, effectively neutralizing them. This results in controlled impurity-band absorption (Sb^0 → CB; Ga^0 → VB), which acts at temperatures below the thermal ionization of the impurities.

2. Experimental

2.1. Germanium crystals

Co-doping of Ge with gradients of antimony and gallium along the crystal has been selected. To obtain a series of germanium samples with different degree of compensation, we used the difference in the distribution coefficients of gallium (0.087) and antimony (0.003) in Ge. Due to the different depletion of Ga and Sb during growth because of the different segregation and diffusion coefficients, both the concentration and the ratio of the impurities vary along the crystal's growth axis. We have modelled the target partial concentration's profiles along the crystal's growth axis (Fig. 2a). The upper limit for the net concentration was targeted to be below $2\bullet 10^{16}$ cm^{-3}, to ensure non-saturated absorbance in the transmission spectra for a sample thickness of about 300 μm. The Ge:Sb:Ga crystals were grown using the Czochralski method. The doping material was introduced directly into the crucible charged with 519 g of polycrystalline Ge. Two crystals were grown with a consequent adding of gallium and antimony. One crystal was aimed to

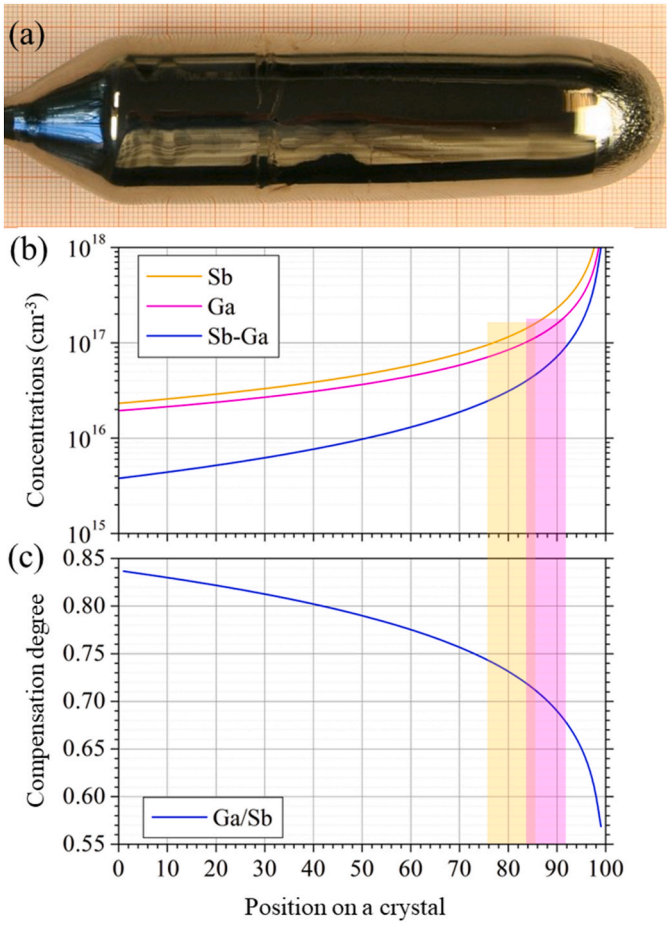


Fig. 2. (a) Image of the *n*-type compensated crystal Ge:Sb:Ga #538. (b) Calculated distribution of the antimony and gallium over the crystal length. (c) Calculated degree of compensation, $k = N_{Ga}/N_{Sb}$. The colored rectangles show the margins of partial critical Mott concentrations for Ga and Sb impurities.

prepare highly compensated *n*-Ge(:Sb:Ga) samples, with a selected volume below N_M and a calculated compensation degree within 75-85% (Ge:Sb:Ga #538) (Fig. 2), the second crystal was designed for highly compensated *p*-Ge(:Ga:Sb) samples, its compensation degree was estimated to vary within 90-100% (Ge:Sb:Ga #539).

Four samples were made from each cut at various positions to the side with the doping level lower than the critical N_M, for the crystal #538 – to the left side (Fig. 2a) of the marked volumes of the critical concentrations.

For optical studies, wedged Ge samples were cut from the cross sections of Ge:Ga:Sb #538 and #539 crystals, and optically polished. The parameters of the samples used are summarized in Table 1.

Table 1
Parameters of the samples used in this study. The partial concentrations were determined from the calculated impurity distribution and the empiric effective net doping, as determined from the measured resistivity. The accuracy of the thickness is within 15 μm.

Sample No	Thickness μm	Wedge	Sb donors, cm^{-3}	Ga acceptors cm^{-3}
HP 40	4510-4960	2.5°	$< 1 \times 10^{13}$	
40D6	5000			$7.8(\pm0.2)\times10^{13}$
471	400-490	1°	$9.1(\pm0.6)\times10^{14}$	
528c	600			$1.(\pm0.1)\times10^{15}$
538.1	540-590	0.29°	$3.3(\pm0.2)\times10^{16}$	$2.9(\pm0.2)\times10^{16}$
538.4	190-360	1.0°	$4.7(\pm0.4)\times10^{16}$	$4.0(\pm0.4)\times10^{16}$
539.1	400-500	0.47°	$2.6(\pm0.2)\times10^{16}$	$2.72(\pm0.2)\times10^{16}$
539.3	300-400	0.57°	$3.4(\pm0.3)\times10^{16}$	$3.3(\pm0.3)\times10^{16}$

2.2. Electrical measurements

Four-point probe resistivity (dedicated setup at IKZ) measurements on the crystal's surface show the approximately expected ranges of net concentrations achieved, within ~10^{14} cm^{-3} - 10^{16} cm^{-3}. The actual net concentration profiles differ from the calculated positions over the crystal' axis. This correction was taken into account when assigning the local partial concentrations and the compensation degree.

Several samples, prepared from the same ingot slices, were processed to obtain lateral Ohmic contacts on their front facets, following a procedure analogous to that described in Ref. [3]. The measured resistance fluctuates within ± 9% around the mean value, which corresponds to the mean resistivity measured via a four-probe technique (Fig. 3).

The temperature evolution of the resistivity was measured on the twin sample (the same slice cut from the Ge crystals was used for both samples: used for electric and for optical measurements) using a dedicated cryogenic probe and a Keithley 2400 source-measure unit. The current-voltage (I-V) dependences follow the net concentrations of free charge carriers; electric breakdown of strongly compensated samples occurs at significantly larger values. The I-V curves show clearly a regime of free carriers freezing onto impurity centers (Fig. 3b); this indicates the existence of at least a ground state as a localized state. The low-temperature resistivity approaches lower values, compared with those for undoped and low-doped Ge samples, - a clear indication of the

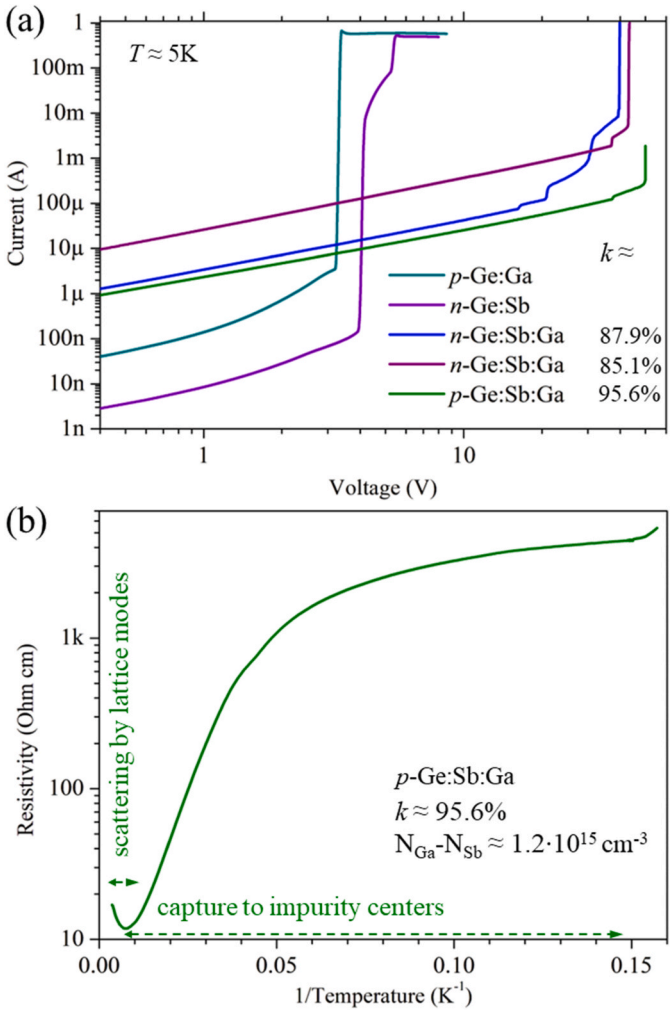


Fig. 3. (a) Low-temperature I-V characteristics of co-doped samples compared to single-dopant *p*-Ge; the samples (top to bottom): 40D6, 471; 538.1, 538.4, 539.1; (b) Temperature dependence of the resistivity of a co-doped, strongly compensated *p*-Ge:Ga:Sb sample # 539.1.

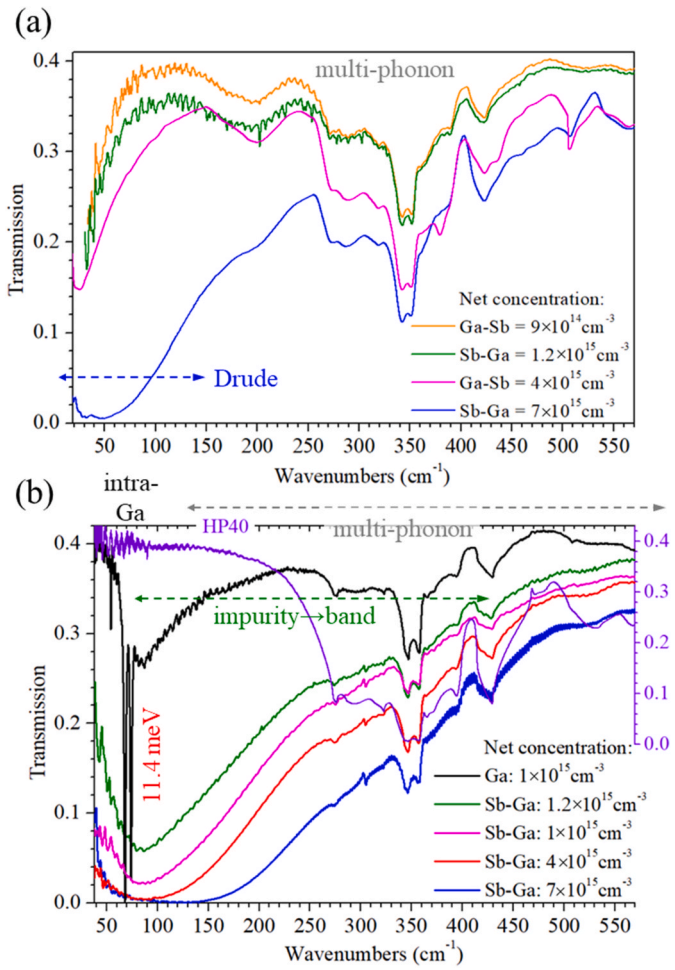


Fig. 4. (a) Room-temperature far-infrared transmission spectra of the co-doped Ge:Sb:Ga samples (top to bottom): 539.3; 539.1, 538.1, 538.4; (b) Low-temperature (T = 5K) spectra, compared to single-dopant Ge:Ga (top to bottom): 528c, 539.1; 539.3, 538.1, 538.4; and a ~5 mm thick high-purity Ge sample (HP 40) with its transmission axis on the right side.

formation of an impurity band arising from merged excited states in moderately doped Ge:Sb:Ga samples, at concentrations exceeding $3\bullet10^{16}$ cm^{-3}.

2.3. Infrared spectroscopy

Infrared spectra were collected with a Bruker Fourier-Transform spectrometer Vertex 80v, at the spectral resolution of 1 cm^{-1}, averaging 211 individual scans, using the sets of beamsplitters and detectors covering a broad spectral range: from 20 cm^{-1} to 8000 cm^{-1}, where the transitions ranging from intracenter and intraband to interband (indirect and direct types, Fig. 1) take place. In the measurements aimed to study influence of optical broad band-gap illumination, the sample compartment in the spectrometer was equipped with thin black polyethylene films (cutoff: above 1200 cm^{-1}). The modulation source used to illuminate samples in the optical cryostat is a tungsten-halogen lamp, type SLS251 (Thorlabs GmbH), with the most spectral density in the near-infrared wavelength range. A 5 mm round spot in the center of the sample facet was irradiated, the estimated integral fluence was 0.7 mW/mm^2. The samples were glued with a conducting paint to a cold finger of a transport liquid helium cryostat. Temperature was monitored via two sensors attached to the cold finger. No temperature change occurred when the measurement was performed under the band-gap illumination.

The far-infrared transmission spectra of highly compensated Ge samples at room temperature (Fig. 4a) reveal low absorption below 150 cm^{-1}, as is to be expected for a highly compensated semiconductor. With increasing net doping, Ge:Sb:Ga samples exhibit a broadband asymmetric absorption that can be plausibly explained by enhanced Drude-like absorption. Other spectral features are typical for intrinsic Ge at room temperature: distinct multi-phonon difference and sum absorption bands (100 – 680 cm^{-1}) and low-frequency slopes similar to those for low-doped germanium, with the absorption values decreasing with increasing compensation degree.

Cooling the compensated *p*-Ge samples results in a significant increase in far-infrared absorption (Fig. 4b). The common absorption band, peaked at about 92 cm^{-1} (11.4 meV), aligns well with the maximum of impurity-band absorption associated with gallium centers (binding energy $E_{Ga} \approx 11.3$ meV [14]), see the spectrum of uncompensated *p*-Ge:Ga (Fig. 4b). At low lattice temperature, the most doped, compensated samples display an additional band in the transmission spectra; the combined absorption is blue-shifted relative to the transitions associated with intracenter and impurity-band absorption; i.e. above the binding energy of gallium or antimony centers, $E_{Sb} \approx$ 10.3 meV, or possible dopant pairs.

The origin of these features is obviously related to the free charge carrier concentrations (both partial and effective net) in the highly doped and compensated germanium. We hypothesize that the extended absorption at temperatures above the impurity ionization threshold may be attributed to the extended tail of the free charge carrier distribution as the Fermi level shifts toward the band edge. The pronounced asymmetry of this absorption band may be a characteristic feature of a tailored distribution into high energies. The rise in absorption at low temperatures (Fig. 5) is directly related to the freeze-out of free carriers. Possible local vibrational modes, associated with antimony, should exhibit narrower spectral lines, impurity-induced one-phonon absorption band should display multiple features spread over a wide spectral range, photoinduced hopping-assisted absorption occurs in a much lower frequency range [15]. Illumination of the samples with a band-gap emission brings additional far-infrared losses (Fig. 5a): tiny (under 1%) at room temperature and significant at temperatures where shallow impurity centers are not completely thermally excited (below 40 K). No temperature change occurred when the measurement was performed under the band-gap illumination. In the latter case, the spectral center of the absorption exhibits a blue shift.

3. Simulation of far-infrared transmission spectra

In order to estimate acting free carrier density, we employed the Drude-Lorentz model for material permittivity, which is known to provide a good approximation for heavily-doped, uncompensated Ge [16]. We express the far-infrared complex permittivity in a general form as follows:

$$\varepsilon(\omega, T) = \varepsilon_\infty - \sum_{i=e,hh} \frac{{\omega_{pi}}^2}{\omega^2 + i\omega\gamma_i} + \sum_{j=ic,ib} \frac{S_j \Gamma_j \omega_{0j}}{\left(\omega_{0j}^2 - \omega^2\right) - i\Gamma_j \omega} + \sum_{lattice} \frac{S_m \Gamma_m \omega_{0m}}{\left(\omega_{0m}^2 - \omega^2\right) - i\Gamma_m \omega} \quad (1)$$

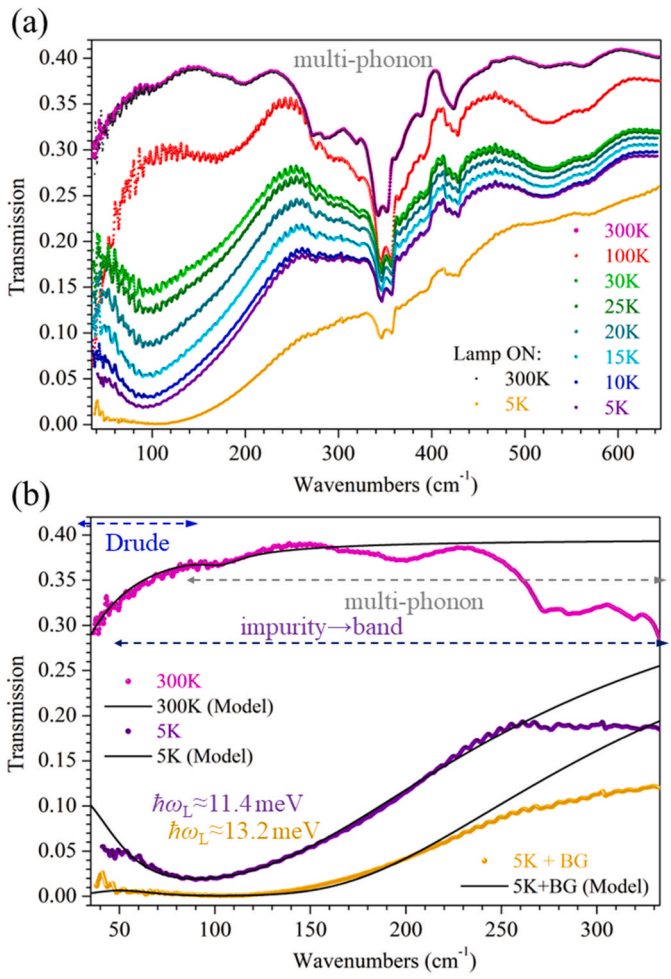


Fig. 5. Temperature dependence of infrared absorption of the co-doped *p*-Ge:Sb:Ga sample #539.3: (a) Transmission in the far-infrared range drops a little under illumination at room temperature, and significantly at 5 K; BG = band-gap illuminated. (b) the Lorentz-Drude model fitting of some spectra in the low-frequency range. Parameters used for the fits: $N_{Ga} \approx 3.60\bullet10^{16}$ cm^{-3}, $N_{Sb} \approx 3.51\bullet10^{16}$ cm^{-3}; $\mu_e = 2030$ cm^2/(Vs), $\mu_e = 1410$ cm^2/(Vs); Lorentzian term parameters of the electronic term (300K/5K/5K + BG): S = 0.0027; $\Gamma = 5\bullet10^{12}$ s^{-1}; $\omega_0 = 1.95\bullet10^{13}$ s^{-1};/S = 3.4; $\Gamma = 2.5\bullet10^{13}$ s^{-1}; $\omega_0 = 1.73\bullet10^{13}$ s^{-1};/S = 5.4; $\Gamma = 2.1\bullet10^{13}$ s^{-1}; $\omega_0 = 2.0\bullet10^{13}$ s^{-1}; the lattice term was adapted from Ref. [8] and implemented only to model the spectrum at 300K.

where the first term is the static permittivity of Ge taken as $\varepsilon_\infty = \varepsilon(\omega\rightarrow\infty; T) = 16$ [17], the second term describes electronic intra(sub)band transitions of free charge carriers (Drude-like absorption), the third term stays for other nonvanishing electronic transitions in this spectral range, namely: intracenter (ic) and impurity → band (ib) transitions (inter-subband transitions in the valence band, heavy-to-light hole, were neglected due to their relatively small cross-section of $< 10^{-17}$ cm^2 in the relevant far-infrared range [18]) and the last term accounts for the contributions of lattice modes. Next, $\omega_{pi}^2 = N_i\bullet e^2\bullet(m_i\bullet\varepsilon_0\bullet\varepsilon_\infty)^{-1}$ are the corresponding Drude weights for $i = \{$electrons; heavy holes$\}$; N_i is the partial density of free charge carriers; e is the elementary charge; m_i is the effective mass of the charge carrier (electrons: $m_e = 0.12\bullet m_0$; heavy holes: $m_{hh} = 0.33\bullet m_0$ [17]); ε_0 is the vacuum permittivity; γ_i are the corresponding damping constants, calculated from empiric values of mobility μ in moderately doped *n*-Ge and *p*-Ge (Refs [19,20]) within the classic Drude model $\gamma = e\bullet(m_{eff}\bullet\mu)^{-1}$ assuming that the number of scattering atoms, determining the mobility of free carriers is equal to the sum $N_{Ga} + N_{Sb}$; S, Γ and ω_0 are the strength, linewidth and center frequencies of the oscillators in the last terms, respectively. For the lattice term, we neglect most contributions from phonon bands in the range $<$ 150 cm^{-1}; except a single, weak, difference-phonon band centered at about 100 cm^{-1} [8]. We also neglect the contributions into the Drude term from the transitions within the light hole and spin-orbit-split sub-bands, as their population are expected to be much smaller compared to those of heavy holes ($4.5\bullet10^{-2}$ and $1.6\bullet10^{-6}$, respectively).

The refractive and extinction coefficients (n(ω,T) and k(ω,T)) are subsequently derived from the permittivity, using the relationship:

$$\varepsilon(\omega,T) = \mathrm{Re}(\varepsilon(\omega,T)) + i\cdot\mathrm{Im}(\varepsilon(\omega,T)) = (n(\omega,T) + i\cdot k(\omega,T))^2$$

Transmission spectra are calculated in the next step, assuming a single path light propagation, valid for the wedged samples used in this study:

$$\mathrm{Trans}(\omega,T) = \left(1 - \left(\frac{n(\omega,T)-1}{n(\omega,T)+1}\right)^2\right)^2 \cdot \exp\left(-4\pi k(\omega,T)d/\lambda\right) \quad (2)$$

We show several specific cases with significantly different transmission spectra (Fig. 5b).

The low-temperature spectrum of a HC *p*-Ge sample (calculated $N_{Ga} \approx 3.4\bullet10^{15}$ cm^{-3}; $N_{Sb} \approx 3.3$; $k \approx 0.97$), assuming no free carriers occurred (the second term in Eq. (1) vanishes to zero), lets a reasonable fitting of the far-infrared region assuming a broadband contribution peaked at about the energy of a Ga center (11.4 meV or ~92 cm^{-1}, the binding energy of a majority impurity, gallium, $E_{Ga} = 11.3$ meV). The corresponding concentration of neutral Ga centers, which would provide the calculated absorption is $1.5^{\pm0.5}\bullet10^{14}$ cm^{-3}, assuming margins for the cross-section at this frequency for moderately doped Ge:Ga [14]. The room temperature spectra of the sample (assuming thermal ionization of shallow impurities occurred, the third term in Eq. (1) vanishes to zero) are well fitted if assuming free charge carriers to be of $9^{\pm1}\bullet10^{14}$ cm^{-3} while the absolute values were taken as $N_{Ga} \approx 3.60\bullet10^{16}$ cm^{-3}, $N_{Sb} \approx 3.51\bullet10^{16}$ cm^{-3} [19,20] in order to match to the empirical values of mobilities for electrons and holes. This slight discrepancy for sample #539.3 suggests two possibilities: (i) the infrared spectra apparently reveal a somewhat lower net doping for the sample from this crystal location than estimated from the resistivity measurements; (ii) the mobility values used in the model are not accurate enough. Note that in the first case, the values taken for modelling the spectra lie within the error margins of the measurement method (Table 1). Both cases of partial concentrations of antimony and gallium yield the compensation in this sample as predicted by simulation, and from electric measurements, $k \approx 97\%$.

Finally, under band-gap excitation at low temperatures, we expect a partial recovering of neutral impurity centers by the subsequent excitation of a valence electron into the conduction band following its capture onto an ionized D^+ donor center. Note, that this capture of a free electron onto the Coulomb center dominates donor-acceptor recombination at low temperatures – the captured electron remains bound to the donor center and contributes to far-infrared absorption. The same, mirrored, process occurred at the acceptor sites. As the result – far-infrared absorption increases. Our fitting yields a fraction of about 8% for recovered (compensated into neutral) Sb and Ga centers, that would quantitively explain the observed slope (Fig. 5b). This picture is consistent with the rates of non-radiative recombination and capture of free carriers known for germanium. For both types of interband recombination – Auger direct and involving localized states within the band gap, rates in the nanosecond-to-microsecond range have been reported at room temperature [21], up to the largest free carrier concentrations (where the recombination rate scales with N^2). Capture into charge impurity atoms at low temperatures occurs on a faster timescale, typical values derived from time-resolved measurements on HDHC *p*-Ge [2] yields characteristic times of less than 100 ps.

Note, that the spectrum width almost remains under the bandgap emission in both spectra at 5 K, while its center exhibits a blue shift towards approximately 13.2 ± 0.1 meV. It can be surmised that this shift manifests the additional rising slope caused by the persistent Drude

absorption – this would imply that a smaller; but detectable part of the photo-induced free charge carriers manages to contribute to the free-carrier far-infrared absorption process complementary to major absorption from the part related to populated ground states of the impurities.

4. Conclusions

Highly compensated (up to 98%), moderately to heavily doped Ge crystals exhibit significant absorption in far-infrared and tailoring into mid-infrared ranges at low temperatures. As the degree of compensation increases, these losses gradually decrease, reaching low levels in highly compensated samples. We selected the regime of the impurity ground states remained isolated and acting as effective Coulomb traps for free charge carriers; interband recombination plays a comparatively minor role. This scenario was realized in high-quality germanium crystals, doped below the Mott transition of gallium and antimony. Far-infrared light transmission was modulated applying a band-gap optical excitation, making this material as a spectrally selective, controllable absorber. The modulation depth is maximized at highest compensation, and can be varied by the fluence of external band-gap illumination. The ultrafast, femtosecond-range scattering between the Γ and L valleys in Ge [22] makes no significant difference in the choice of the modulating source; its wavelength merely needs to be shorter than those corresponding to the indirect band gap of germanium. The net concentrations were found to determine both electric and optical characteristics and point on approximately the same values for the measured samples. The HDHC Ge crystals remain transparent into the lowest frequencies in these measurements, indicating low-moderate Drude loss and apparent preventing role of compensation in the formation of surface and bulk plasmons.

CRediT authorship contribution statement

S.G. Pavlov: Writing – review & editing, Writing – original draft, Project administration, Methodology, Investigation, Formal analysis, Data curation, Conceptualization. **N.V. Abrosimov:** Writing – review & editing, Validation, Resources, Methodology, Investigation. **D.L. Kamenskyi:** Writing – review & editing, Writing – original draft, Validation, Investigation, Funding acquisition, Formal analysis. **H.-W. Hübers:** Writing – review & editing, Supervision, Resources, Project administration, Conceptualization.

Declaration of competing interest

The authors declare that they have no known competing financial interests or personal relationships that could have appeared to influence the work reported in this paper.

Acknowledgements

The authors thank the financial support from the German Research Foundation (Deutsche Forschungsgemeinschaft) under DFG project number 509105207.

Data availability

Data will be made available on request.

References

[1] A. Cuevas, M. Forster, F. Rougieux, D. Macdonald, Compensation engineering for silicon solar cells, Energy Proc. 15 (2012) 67–77, https://doi.org/10.1016/j.egypro.2012.02.008.
[2] N. Deßmann, S.G. Pavlov, A. Pohl, N.V. Abrosimov, S. Winnerl, M. Mittendorff, R. Kh Zhukavin, V.V. Tsyplenkov, D.V. Shengurov, V.N. Shastin, H.-W. Hübers, Lifetime-limited, subnanosecond terahertz germanium photoconductive detectors, Appl. Phys. Lett. 106 (2015) 171109, https://doi.org/10.1063/1.4918712.
[3] S.G. Pavlov, N. Deßmann, A. Pohl, N.V. Abrosimov, M. Mittendorff, S. Winnerl, R. Kh Zhukavin, V.V. Tsyplenkov, D.V. Shengurov, V.N. Shastin, H.-W. Hübers, Towards a life-time-limited 8-octave-infrared photoconductive germanium detector, J. Phys.: Conf. Ser. 647 (2015) 012070, https://doi.org/10.1088/1742-6596/647/1/012070.
[4] S. Zh. Karazhanov, Properties of precisely compensated semiconductors, Semicond 34 (8) (2000) 872–879, https://doi.org/10.1134/1.1188091.
[5] V.V. Parshin, R. Heidinger, B.A. Andreev, A.V. Gusev, V.B. Shmagin, Silicon as an advanced window material for high power gyrotrons, Int. J. Infrared and Millimeter Waves 16 (1995) 863–877, https://doi.org/10.1007/BF0206666277.
[6] S. Zwerdling, J.P. Theriault, Far infrared spectral properties of compensated Ge and Si, Infrared Phys. 12 (3) (1972) 165–186, https://doi.org/10.1016/0020-0891(72)90041-3.
[7] E. Bründermann, H.-W. Hübers, M.F. Kimmitt, in: Terahertz Techniques, Springer Series in Optical Sciences, 151, Springer, Berlin, Heidelberg, 2012, https://doi.org/10.1007/978-3-642-02592-1.
[8] M. Ikezawa, T. Nanba, Two-Phonon difference absorption spectra in Ge crystals, J. Phys. Soc. Jpn. 45 (1978) 148–152, https://doi.org/10.1143/JPSJ.45.148.
[9] B.I. Shklovskii, A.L. Efros, Completely compensated crystalline semiconductor as a model of an amorphous semiconductor, Sov. Phys. JETP 35 (3) (1972) 610–614. https://www.jetp.ras.ru/cgi-bin/dn/e_035_03_0610.pdf.
[10] M.N. Alexander, D.F. Holcomb, Semiconductor-to-Metal Transition in *n*-Type Group IV semiconductors, Rev. Mod. Phys. 40 (1968) 815–829, https://doi.org/10.1103/RevModPhys.40.815.
[11] T.F. Rosenbaum, R.F. Milligan, M.A. Paalanen, G.A. Thomas, R.N. Bhatt, W. Lin, Metal-insulator transition in a doped semiconductor, Phys. Rev. B 27 (1983) 7509–7523, https://doi.org/10.1103/PhysRevB.27.7509.
[12] H. Fritzsche, The metal–nonmetal transition in disordered systems, in: L. R. Friedman, D.P. Tunstall (Eds.), Proc.19th Scottish Universities Summer School in Physics,, 1978, p. 193. St. Andrews, UK.
[13] K.M. Itoh, M. Watanabe, Y. Ootuka, E.E. Haller, T. Ohtsuki, Complete scaling analysis of the metal–insulator transition in Ge:Ga: effects of doping-compensation and magnetic field, J. Phys. Soc. Jpn. 73 (1) (2004) 173–183, https://doi.org/10.1143/JPSJ.73.173.
[14] R.L. Jones, P. Fisher, Excitation spectra of group III impurities in germanium, J. Phys. Chem. Solid. 26 (7) (1965) 1125–1131, https://doi.org/10.1016/0022-3697(65)90008-9.
[15] H.F. Jang, G. Cripps, T. Timusk, Far-infrared absorption of neutron-transmutation-doped germanium, Phys. Rev. B 41 (1990) 5152–5168, https://doi.org/10.1103/PhysRevB.41.5152.
[16] J. Frigerio, A. Ballabio, G. Isella, E. Sakat, G. Pellegrini, P. Biagioni, M. Bollani, E. Napolitani, C. Manganelli, M. Virgilio, A. Grupp, M.P. Fischer, D. Brida, K. Gallacher, D.J. Paul, Tunability of the dielectric function of heavily doped germanium thin films for mid-infrared plasmonics, Phys. Rev. B 94 (2016) 085202, https://doi.org/10.1103/PhysRevB.94.085202.
[17] M. Levinshtein, S. Rumyantsev, M. Shur (Eds.), Handbook Series on Semiconductor Parameters, 1, World Scientific Publishing Co. Pte. Ltd., Singapore, 1996, https://doi.org/10.1142/2046-vol1.
[18] Yu. K. Pozhela, E.V. Starirov, P.N. Shiktorov, Far infrared absorption by hot holes in p-Ge, Phys. Stat. Sol. (b) 128 (1985) 653–661, https://doi.org/10.1002/pssb.2221280231.
[19] O.A. Golikova, B.Ya. Moizhez, L.S. Stilbans, Hole mobility of germanium as a function of concentration and temperature, Sov. Phys. Solid State 3 (1962) 2259–2265.
[20] V.I. Fistul, M.I. Iglitsyn, E.M. Omelyanovskii, Mobility of electrons in germanium strongly doped with arsenic, Sov. Phys. Solid State 4 (1962) 784–785.
[21] P. Martín, A. Cano, I. García, I. Rey-Stolle, Review of intrinsic vs. extrinsic recombination in germanium thermophotovoltaic converters, Sol. Energy Mater. Sol. Cells 291 (2025) 113741, https://doi.org/10.1016/j.solmat.2025.113741.
[22] X.Q. Zhou, H.M. van Driel, G. Mak, Femtosecond kinetics of photoexcited carriers in germanium, Phys. Rev. B 50 (1994) 5226–5230, https://doi.org/10.1103/PhysRevB.50.5226.